Geochemistry Geophysics Geosystems G3

Published by AGU and the Geochemical Society

Article
Volume 11, Number 5
11 May 2010
Q05S23, doi:10.1029/2009GC002844
ISSN: 1525-2027

Click Here for Full Article

Tephra layers: A controlling factor on submarine translational sliding?

Rieka Harders, Steffen Kutterolf, and Christian Hensen
SFB 574, Leibniz-Institut für Meereswissenschaften an der Universität Kiel (IFM-GEOMAR), Wischhofstrasse 1-3, D-24148 Kiel, Germany (rharders@ifm-geomar.de; skutterolf@ifm-geomar.de; chensen@ifm-geomar.de)

Tobias Moerz
MARUM, Leobener Strasse, D-28359 Bremen, Germany (tmoerz@uni-bremen.de)

Warner Brueckmann
Leibniz-Institut für Meereswissenschaften an der Universität Kiel (IFM-GEOMAR), Wischhofstrasse 1-3, D-24148 Kiel, Germany (wbrueckmann@ifm-geomar.de)

[1] Submarine slope failures occur at all continental margins, but the processes generating different mass wasting phenomena remain poorly understood. Multibeam bathymetry mapping of the Middle America Trench reveals numerous continental slope failures of different dimensions and origin. For example, large rotational slumps have been interpreted to be caused by slope collapse in the wake of subducting seamounts. In contrast, the mechanisms generating translational slides have not yet been described. Lithology, shear strength measurements, density, and pore water alkalinity from a sediment core across a slide plane indicate that a few centimeters thick intercalated volcanic tephra layer marks the detachment surface. The ash layer can be correlated to the San Antonio tephra, emplaced by the 6000 year old caldera-forming eruption from Masaya-Caldera, Nicaragua. The distal deposits of this eruption are widespread along the continental slope and ocean plate offshore Nicaragua. Grain size measurements permit us to estimate the reconstruction of the original ash layer thickness at the investigated slide. Direct shear test experiments on Middle American ashes show a high volume reduction during shearing. This indicates that marine tephra layers have the highest hydraulic conductivity of the different types of slope sediment, enabling significant volume reduction to take place under undrained conditions. This makes ash layers mechanically distinct within slope sediment sequences. Here we propose a mechanism by which ash layers may become weak planes that promote translational sliding. The mechanism implies that ground shaking by large earthquakes induces rearrangement of ash shards causing their compaction (volume reduction) and produces a rapid accumulation of water in the upper part of the layer that is capped by impermeable clay. The water-rich veneer abruptly reduces shear strength, creating a detachment plane for translational sliding. Tephra layers might act as slide detachment planes at convergent margins of subducting zones, at submarine slopes of volcanic islands, and at submerged volcano slopes in lakes.

Components: 9600 words, 14 figures, 1 table.

Keywords: submarine landslides; mass wasting; ash layers; liquefaction; translational sliding; permeability.

Index Terms: 3070 Marine Geology and Geophysics: Submarine landslides (1031); 3060 Marine Geology and Geophysics: Subduction zone processes (1031).

Received 11 September 2009; **Revised** 23 February 2010; **Accepted** 23 March 2010; **Published** 11 May 2010.

Harders, R., S. Kutterolf, C. Hensen, T. Moerz, and W. Bruekmann (2010), Tephra layers: A controlling factor on submarine translational sliding?, *Geochem. Geophys. Geosyst.*, *11*, Q05S23, doi:10.1029/2009GC002844.

Theme: Central American Subduction System
Guest Editors: G. Alvarado, K. Hoernle, and E. Silver

1. Introduction

[2] Along the Middle America Trench, slope failure has been related to (1) subduction of large seamounts [e.g., *von Huene et al.*, 2000, 2004] and (2) widespread tectonic erosion removing material from the lower part of the overriding plate [*Ranero and von Huene,* 2000; *Ranero et al.*, 2008]. Multibeam bathymetry along ~600 km of the continental slope of Costa Rica and Nicaragua displays abundant large slope failures (a failure every ~20 km) occurring as rotational slumps or translational slides of different dimensions (Figure 1). The age of the slides calculated by estimating the time required filling the deepest scars by sediment accumulation rates of 30–40 cm kyr^{-1} after *Kutterolf et al.* [2008c], ranges between at least 500 ka and present.

[3] The mechanisms involved in bedding-parallel translational slides imply the presence of bedding planes containing discrete weak layers because the movement of the failing sediment takes place along the stratification [*Hampton and Lee,* 1996]. By contrast, rotational slumps can occur in homogenous sediments, where a listric rupture surface forces them to rotate along this surface [*Mulder and Cochonat,* 1996]. Slides and slumps can be morphologically classified using the value of the Skempton ratio t/l, where t is the slide thickness and l the slide length. Translational slides usually have Skempton ratios <0.15 and rotational slumps >0.33 with a transition range between 0.15 and 0.33 [*Skempton and Hutchinson,* 1969].

1.1. Seamount Subduction

[4] Offshore Costa Rica large seamounts 2–4 km tall and ~20 km wide underthrust the continental margin. As the seamounts underthrust and subduct under the continental margin, large rotational slumps, 50–60 km lateral width and 50 ≤ 600 m headwalls, collapse in their wakes. Seamount-related mass wasting creates grooves in the slope, caused by the landward retrogression of the headwalls [*von Huene et al.*, 2004]. Bedding planes apparently do not control the movement of large seamount-induced rotational slumping because in many cases the slump involves the basement rock. In contrast, offshore Nicaragua, where smaller seamounts (0.5–2 km high) and lower relief horsts and grabens enter the subduction zone, the presence of large translational slides with 10–12 km long slide planes, 5–6 km lateral width and up to 250 m headwalls, indicates the existence of controlling weak bedding planes (Figure 1). Although deep penetration seismic reflection data have shown that subducting seamounts may also be involved in the generation of the large sediment failures offshore Nicaragua [*McIntosh et al.*, 2007], the slide scars in the slope exhibit an unexplained translational rather than rotational character.

[5] Seismic activity between Costa Rica and Nicaragua causes frequent large earthquakes. *Ambraseys and Adams* [1996] have shown that there have been at least five earthquakes with $M_s > 7$ since 1898, two of which caused tsunamis. The latest $M_s > 7$ earthquake in 1992 caused the tsunami that produced the highest damage along the coast of Nicaragua. Multibeam bathymetry data collected subsequently revealed the presence of large submarine scars in the slope offshore Nicaragua [*von Huene et al.*, 2000], which led to a discussion concerning a potential generation of the tsunami by the submarine slides. *von Huene et al.* [2004] tested the tsunamigenic potential of the largest translational slides offshore Nicaragua located near the epicenter of the 1992 earthquake. They calculated that the slide may have caused a water layer deformation with a maximum amplitude of 6.6 m, causing a tsunami that could potentially affect about 40 km of the Nicaraguan coast, but they could not find any evidence that the slope failures occurred during the 1992 earthquake.

1.2. Slope Stability and Trigger Mechanisms for Translational Sliding

[6] *Spangenberg* [2002] estimated slope stability nearby the largest translational slides offshore Nicaragua by calculating a Safety Factor (SF). He calculated a SF for static and dynamic conditions from piston and box core samples of the clayey deposits collected during R/V *Sonne* cruise 107.

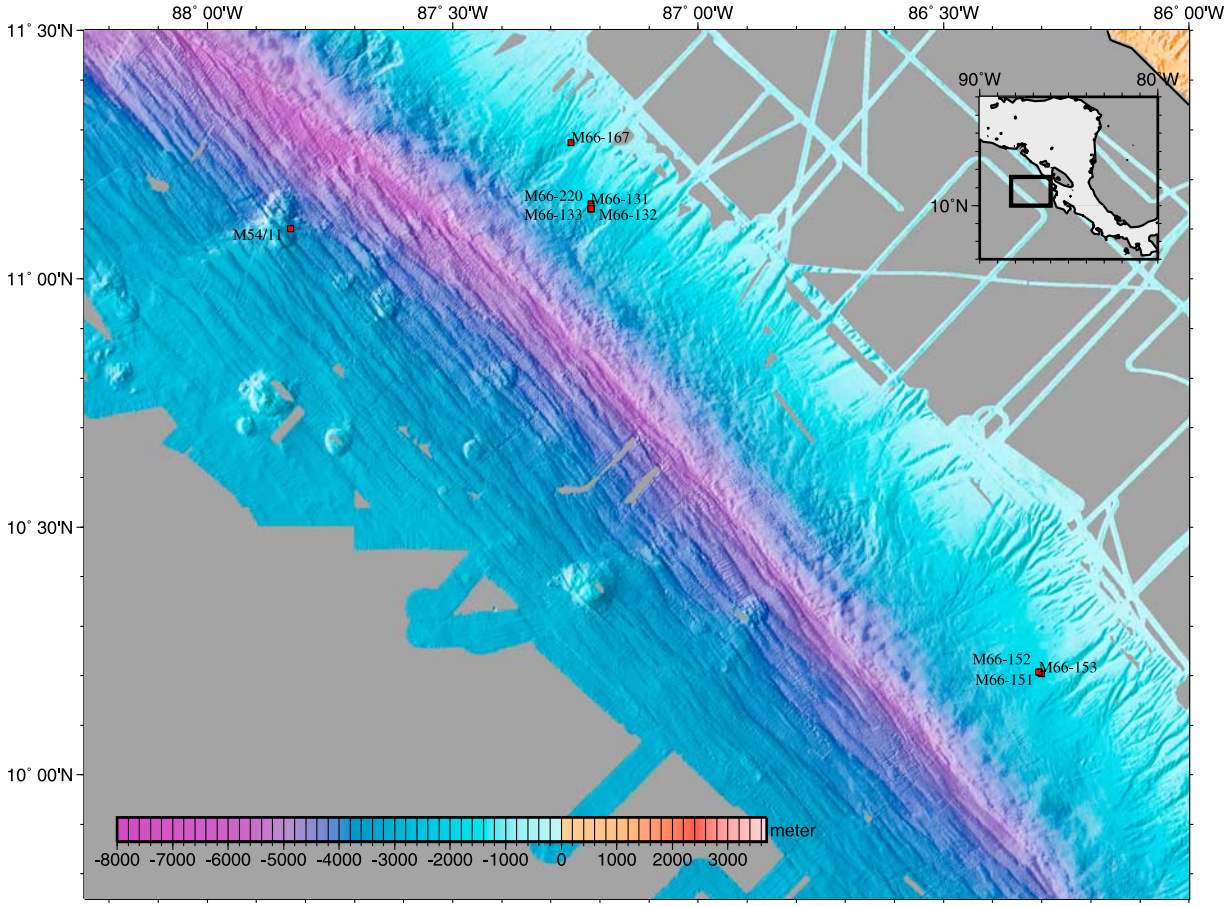

Figure 1. Shaded relief map offshore Central America. Bathymetry data are color coded from pale blue to dark blue. Numbers refer to cores taken with German research vessel *Meteor* cruises M54 and M66 and German research vessel *Sonne* cruise SO 107. Cores 131–133 were taken at Masaya slide, a big slide scar of 12 km × 6 km. Numbers 151–153 refer to cores taken at the medium-sized Hermosa slide (scar of 3 km × 7 km), with core 151 discussed in section 3.2.

For undrained, static conditions, he used the SF formula and method after *Graham* [1984] where

$$SF = \mathrm{cu}/j' h(\sin i \cos i) \quad (1)$$

(with cu = undrained shear strength, j′ = relative bulk density (expressed as the difference between bulk density and the water density), h = sediment thickness between seafloor and slide plane, i = slope angle) and calculated values between 5 to 30, indicating a stable slope. For undrained, dynamic conditions, he used the procedure after *Karlsrud and Edgers* [1982] with the formula

$$SF = \mathrm{cu}/\left(\mathrm{j}'\mathrm{h}\left((1/2)\sin 2i + a\left(\mathrm{j}/\mathrm{j}'\cos^2 i\right)\right)\right) \quad (2)$$

(with j = wet bulk density and a = horizontal ground acceleration earthquakes) assuming earthquake shaking with magnitudes >4.5, (linked to a peak ground acceleration of 0.3 m s^{-2}), and slope angles >12°. Under these conditions SF is close to 1, implying that the slope is prone to failure. However, like in many other studies, these estimations did not account for stratification of the slope sediment and the potentially different mechanical behaviors of the layers, which may enhance the potential for translational sliding. In particular both, the nature of the detachment plane and the failure mechanism causing translational sliding have not yet been investigated.

[7] Here we examine the importance of ash layers as heterogeneities in the otherwise typically terrigenous and pelagic slope sediment sequences and their potential role in slope stability. Tephra layers are formed by pyroclastic matter from explosive volcanic eruptions that disperse material at stratospheric heights and are common horizons in the sediment record offshore Pacific Central America [*Kutterolf et al.*, 2007a, 2007b]. Stratified soil containing layers of different grain size, and therefore different permeability, has been the focus of research dealing with liquefaction and slope

stability since the late 1960s [*Castro,* 1969]. Intensive laboratory work has been performed to study the behavior of stratified soil and the buildup of water films sandwiched between less permeable soil, and liquefied sand, potentially triggering slides.

[8] *Kokusho* [2003] has tested lateral flow failure initiated by earthquake shaking with laboratory shake table tests and demonstrated that void redistribution in sand deposits creates water films if low-permeability layers are present that trap the water films beneath them. *Field et al.* [1982] investigated the submarine failure that occurred during the 1980 earthquake offshore California on the Klamath River and could clearly relate it to a submarine liquefaction phenomenon. However, most liquefaction studies were conducted in subaerial conditions.

[9] In our study we present a new model of liquefaction of ash layers in the submarine environment offshore Nicaragua. Here, we have found 1 to 15 cm thick tephra layers interlayered roughly every 1 m, between marine clays, to be potential weak layers. We propose that ash layers may partially liquefy during earthquake shaking, building up water films sandwiched between the less permeable clay, and finally leading to translational sliding.

2. Methods

2.1. Seafloor Mapping

[10] Multibeam bathymetry data were collected during German R/V *Sonne* cruises SO76, 81, 107, 144, 150, 163-1 and U.S. R/V *M. Ewing* cruises 0005 and 01404 using the Atlas Hydrosweep system and *Sonne* 173 cruise using the SIMRAD EM-120 system from Krongsberg. Water velocity profiles we calculated from CTD measurements. The bathymetric data were cleaned and converted to depth soundings with the MBsystem [*Caress and Chayes,* 1996] and gridded with GMT [*Wessel and Smith,* 1998] at 0.001 degrees node spacing.

2.2. Core Location, Positioning, and Gravity Core Recovery

[11] Gravity cores were 6–9 m long steel tubes filled with a 10 cm wide inner PVC liner. Core locations were planned using Multibeam bathymetry maps and Parasound profiles, shot perpendicular to the headwall of the slides. Cores were positioned in the slide scar close to the headwall and also in undisturbed sediments upslope of the headwall. Positioning during coring was controlled by on board GPS and simultaneous Parasound images. Due to weak rope tension of the core device at water depths >1000 m derivations from the planned position may be up to ~250 m (E. Stehn, technical assistant, R/V *Meteor* cruise M66/3a, personal communication, 2006). Recovered cores were cut into 1 m segments, locked at both sides and stored at 4°C. Measurements were taken within less of 1 h.

2.3. Sediment Analysis

[12] Core segments were analyzed with the GEOTEK Ltd. multisensor whole core logger (MSCL) [*Blum,* 1997], for the data used in this study. Core segments were described, photographed, sampled for pore water chemistry, moisture content, mineral density, and additionally undrained shear strength was measured. Pore water was retrieved by pressure filtration. For further information see http://www.ifm-geomar.de/index.php?id=mg_analytik. Moisture content and mineral density were determined through mass and volume determinations [*Blum,* 1997], measuring the specimen's mass before and after removal of interstitial pore fluid through oven drying for 24 h at temperatures from 90° to 110°C. Moisture content, porosity, and void ratio are defined by the mass or volume of extracted water, corrected for the mass and volume of salt evaporated during the drying, following ODP procedures [*Blum,* 1997]. Undrained shear strength was determined with a fall cone penetrometer, and calculated after *Hansbo* [1957] with the coefficients from *Houlsby* [1982].

2.4. Shear Tests

[13] To measure total displacement, shear strength and compaction of ash layers under a load and during a shear event, dry mono grain size ashes and combinations of different grain sizes were loosely put into a shear box of a direct shear test device following the indications given by *Deutsches Institut für Normung* [2002]. For the tests, grain sizes of cored ash layers were determined by wet sieving or by a laser particle analyzer. A volume of ~100 cm^3 in the shear box was loaded with 16 kg, producing an effective vertical stress of 40 kPa, similar to vertical stress existing at 7 m depths bsf. Shearing in one direction started after 10 min of preconsolidation with a velocity of 0.5 mm min^{-1} until residual shear strength was reached and put to reverse with the same velocity back to the starting point. Sharing went on until no significant changes in peak shear strengths were detected (at least 4 rounds).

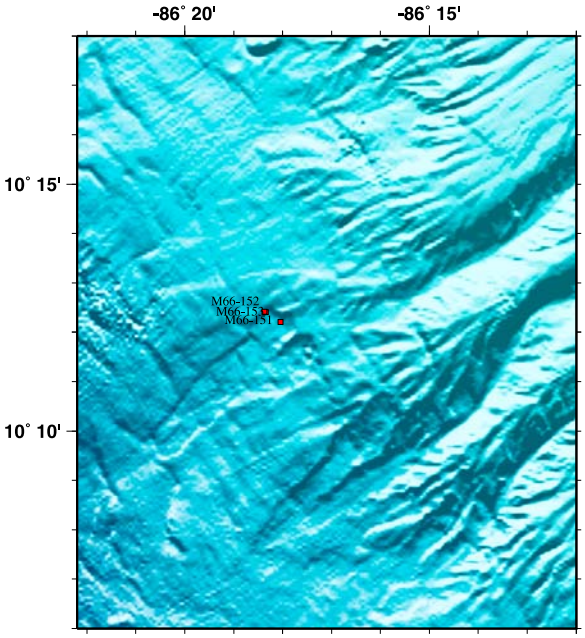

Figure 2. Shaded relief map offshore Costa Rica showing Hermosa slide (scar of 3 km × 7 km), with core locations (red squares) M66/151 to M66/153 in the northwest of the upper slide scarp.

2.5. Ash Layer Chemistry and Correlation

[14] Marine ash beds and matrix glass of onshore samples were analyzed by electron microprobe (EMP) for major and minor elements at IFM-GEOMAR, Kiel as well as Laser ablation inductively coupled mass spectrometry (La-ICP-MS) at University of Frankfurt am Main (Institute of Mineralogy). Standard deviation is less than 2% for major elements and <10% for tracer elements. All analyses have been normalized to 100% to eliminate the effects of variable postdepositional hydration from the comparison between marine and/or on-land tephras [*Kutterolf et al.*, 2008a]. For age determination volcanic offshore ashes were chemically correlated with on land deposits [*Kutterolf et al.*, 2008a].

3. Observations

3.1. Translational Slides and Material at the Slide Plane

[15] Morphologically, scarps caused by translational slides offshore Nicaragua and the northwestern part of Costa Rica have a short headwall area that grows retrogressively upslope, and relatively long converging side flanks (Figures 1–4). The retrogressive character indicates that the original slide causes secondary slides. The secondary events are typically smaller than the main event.

[16] Interpretation of side scan sonar and bathymetry data indicates that most headwalls possibly developed at trench parallel fault scarps (Figure 5). Seafloor offsets by faulting are up to 200 m within the steep (12–17°) middle slope, and the maximum thicknesses of the slides and their headwall, range from 25 to 200 m. The minimum runouts are 1.5 to 12 km, implying Skempton ratios <0.15 that typically characterize translational slides. But many slides have no identifiable deposits because they seem to have run into the trench axis.

[17] Most of the material involved in the slides is hemipelagic to turbididic terrigenous slope sediment that mainly consists of clay with abundant foraminifers [*Spangenberg,* 2002; *Kutterolf et al.*, 2008a]. In general the grain size of these sediments is smaller than 32 μm, which implies that they have low specific hydraulic conductivities (k_f values) of around $<1 \times 10^{-9}$ m s^{-1} [*Hoelting and Coldewey,* 2009] and cohesive properties. The k_f value is given within Darcy's law as

$$k_f = Q/(A*i) \quad (3)$$

with Q (units of volume per time in m^3 s^{-1}), A (cross-sectional area to flow in m^2), and i (dimensionless hydraulic gradient defined as h/l, describing the pressure drop (h) and over a certain length (l)).

[18] These none conductive slope sediments are interlayered every ~1 m with 1–15 cm thick ash layers. The grain size of those discrete ash layers ranges between 63 and 500 μm (silt to sand size), which implies that they have higher hydraulic conductivities and noncohesive properties, compared to the terrigenous slope sediment.

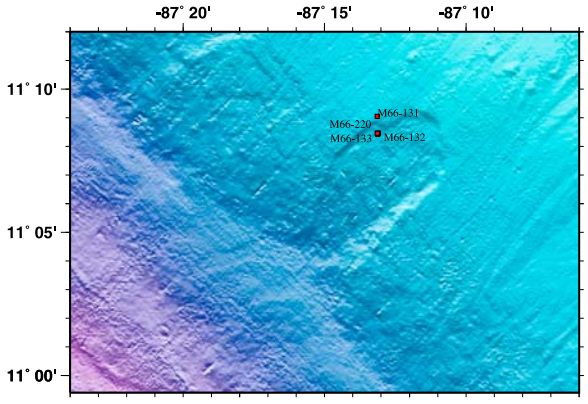

Figure 3. Shaded relief map offshore Nicaragua, showing core locations M66/131 to M66/133, taken at Masaya slide (slide scar 12 km × 6 km).

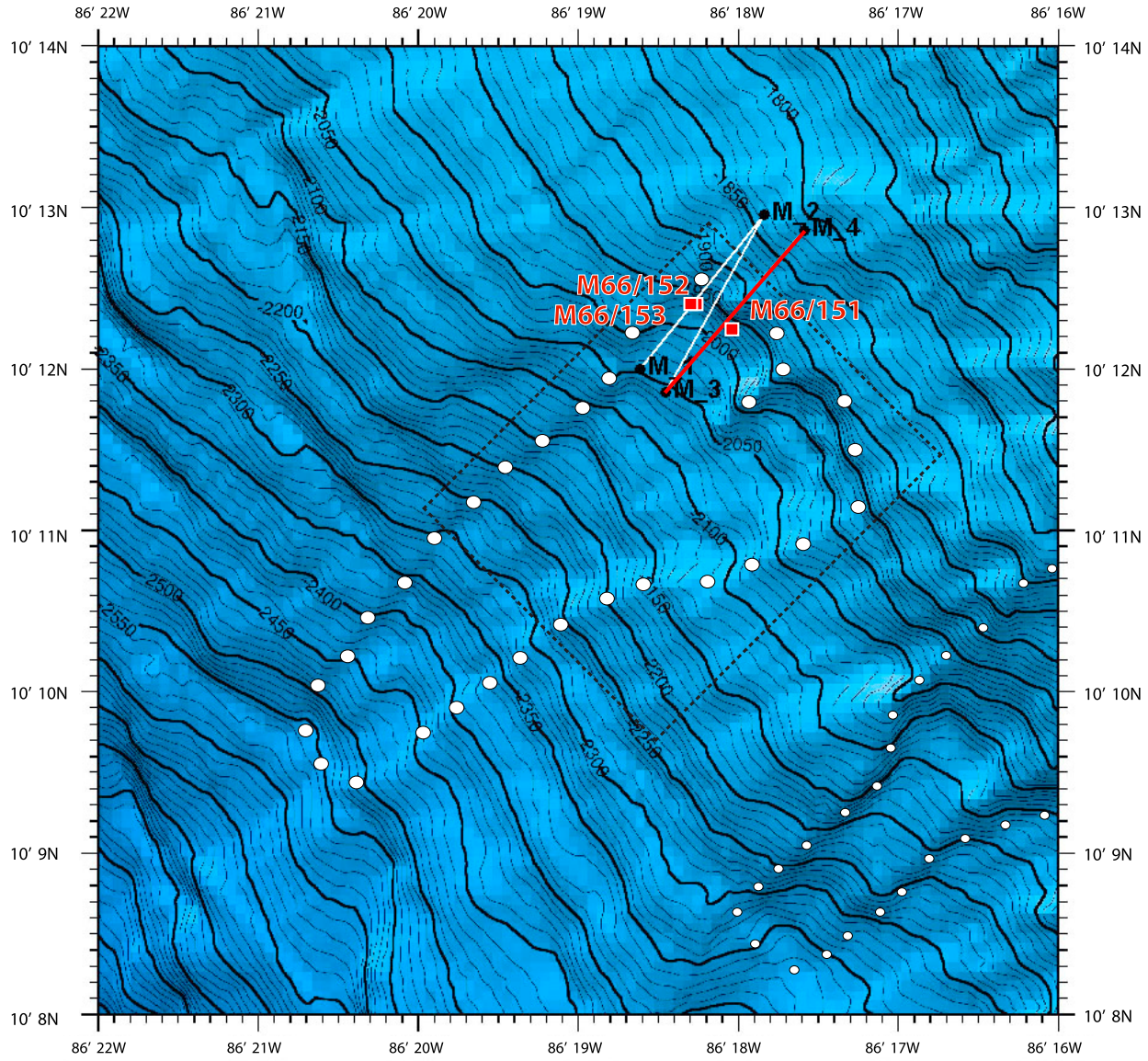

Figure 4. Multibeam bathymetry map of Hermosa slide with contour lines every 10 m. The slide and a near by similar feature are delineated by white filled black circles. Locations of gravity cores M66/151, M66/152, and M66/153 are marked with red squares. Subbottom seismic profiler parasound track is indicated by lines across the headwall (M1–M4 are navigation waypoints). The seismic image from the red track is shown in Figure 6. Black dashed box shows the location of side scan sonar data shown in Figure 5.

3.2. Translational Hermosa Slide

[19] To study translational sliding, R/V *Meteor* cruise 66 targeted several slope failures offshore Costa Rica and Nicaragua. Prior to coring, subbottom profile images were collected with the Parasound system across the headwall area of each of the chosen slides to determine the coring locations. Here we focus on the medium-sized Hermosa scarp (Figure 2), where coring succeeded to penetrate the slide plane.

[20] The scarp extends from 1900 to 2500 m water depth, with a headwall height of about 25 m, and a headwall dip of 12.7°. The undisturbed slope next to the slide has an average dip of 5.7°, lower than the slope dip angles next to most other large translational slides (12–17°) offshore Nicaragua, e.g., Masaya slide (Figure 3).

[21] Parasound images across the headwall and upper first kilometer of the slide plane show the upper tens of meters of the sediment sequence

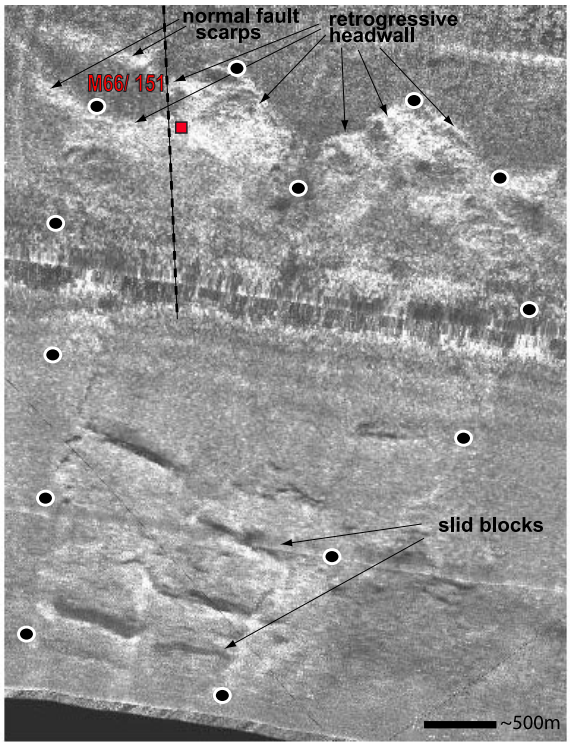

Figure 5. TOBI side scan data of the upper region of the Hermosa slide. Dots (black, encircled in white) mark the outline of the slide. Arrows point to the retrogressive character of the headwall and slid blocks on the slide plane as well as to normal fault scarps in the slopes sediment. Core position M66/151 (marked as red square) is located where slide plane and headwall merge. The location of the Parasound profile (Figure 6) is marked as a black dashed line. Location is shown in Figure 4 as black dashed box.

(Figure 6). Disturbed layers (water depth >2000 m) are visible below the headwall, and in the slide plane. Stratified layers above the headwall appear as parallel reflections and are interpreted as the undisturbed slope sediment. The bathymetry and side scan sonar data show that the headwall area of Hermosa slide consists of two concave shaped headwalls, separated by a central ridge (Figure 2, 4, and 5). The sidewalls of the scar slightly converge and terminate in a tongue-shaped foot of the scar about 7 km downslope from the headwall (Figure 2, 4, and 5). However, most of the displaced mass lies as large block or sheet deposits on the scar plane, which is visible in the Parasound image (Figure 6) and side scan sonar data (Figure 5). The Slide sediments also contain cracks and fissures. Like for most translational slides offshore Nicaragua and Costa Rica, a lobe of sediment accumulation is not observed at the toe of the scar (Figures 2 and 3). *Spangenberg* [2002] and *von Huene et al.* [2004] interpreted this to be related to translational sediment blocks disintegration into density flows. However, at Hermosa slide, side scan sonar data indicate that much of the deposits remain within the slide area, mostly in the upper part of the slide. In order to penetrate through the deposits into the slide plane, the uppermost region of the slide scarp was selected for coring, where the slide sediments are generally thinner.

[22] Attempts to penetrate the slide plane at the large Masaya slide with cores M66/131, M66/132, M66/133 and M66/220 were unsuccessful (Figures 1 and 3). These cores recovered reworked brown to grayish silty clays with few intercalations of mafic or felsic ash layers, which were analyzed geochemically and subsequently used for tephra stratigraphy [*Kutterolf et al.*, 2008a]. Core M66/151 succeeded to sample across the uppermost area of the scar at the smaller Hermosa slide (Figures 1, 2, and 4–6), at a location immediately beneath the headwall, in the upper northwestern part of the scar (Figures 4–6).

[23] Since there was only a thin sediment cover on top of the slide plane it was possible to recover a distinct transition through undisturbed young sediments, slide deposits, a slide plane and the shallowest portion of undisturbed older material within a 3 m long gravity core.

[24] Evidence that a slide plane was reached during coring is supported by all data obtained from the analysis of the core. The MSCL density data, porosity and undrained shear strength laboratory data, as well as pore water alkalinity of the core, show an abrupt change between 1.40 and 1.70 m below seafloor (bsf) (Figure 7), across a coarse-grained 0.5 cm thick mafic ash layer that separates two sediment units. A 10 cm thick layer of reworked material containing finer grained ash clasts as well as rounded mud clasts overlying the 0.5 cm thick coarse ash layer also supports this interpretation (Figure 7).

[25] Above and below ~170 cm bsf the pore water alkalinity profile taken from the core shows two different linear trends, forming a so-called "kink-type" curve, which can be interpreted as the result of a slide event [*Zabel and Schulz,* 2001; *Hensen et al.*, 2003]. Within undisturbed marine sediment alkalinity is typically continuously increasing with increasing sediment depth due to ongoing biodegradation processes. A kink or discontinuity in a pore water profile, as observed in this case, usually

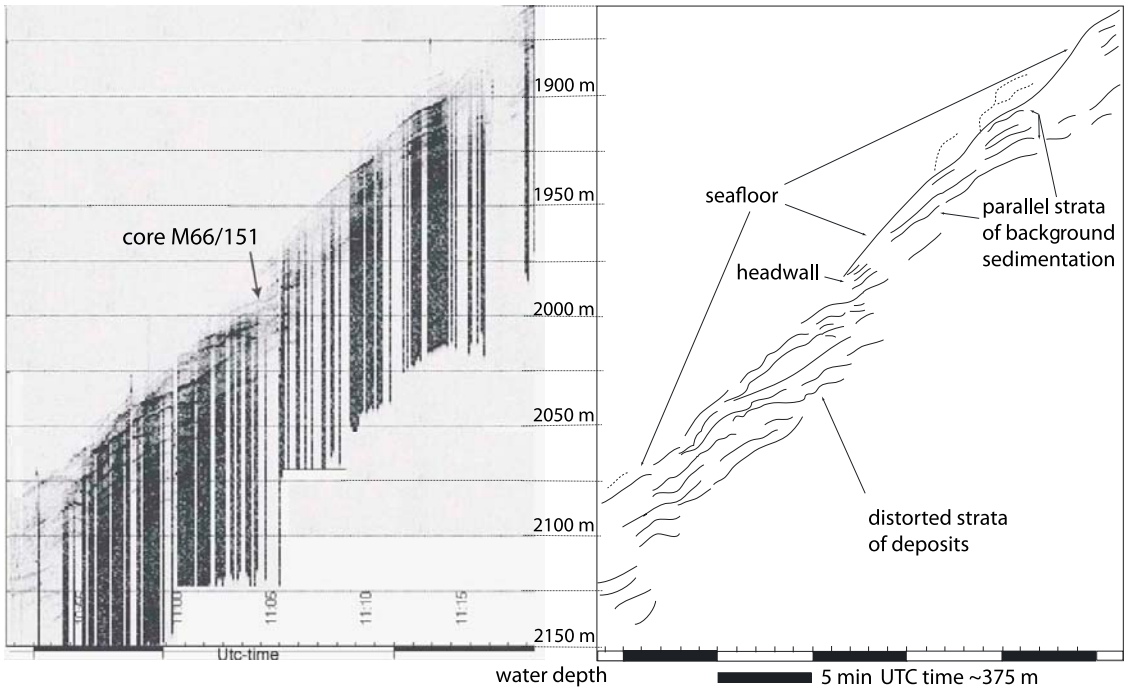

Figure 6. Parasound subbottom seismic profiler image and line interpretation across the headwall of Hermosa slide (see profile location in Figure 4 marked as red line). In spite of interferences with the signal of other instruments shown as black stripes in the image the strata and headwall scarp are clearly visible. Five minutes of UTC time ~375 m on *x* axis.

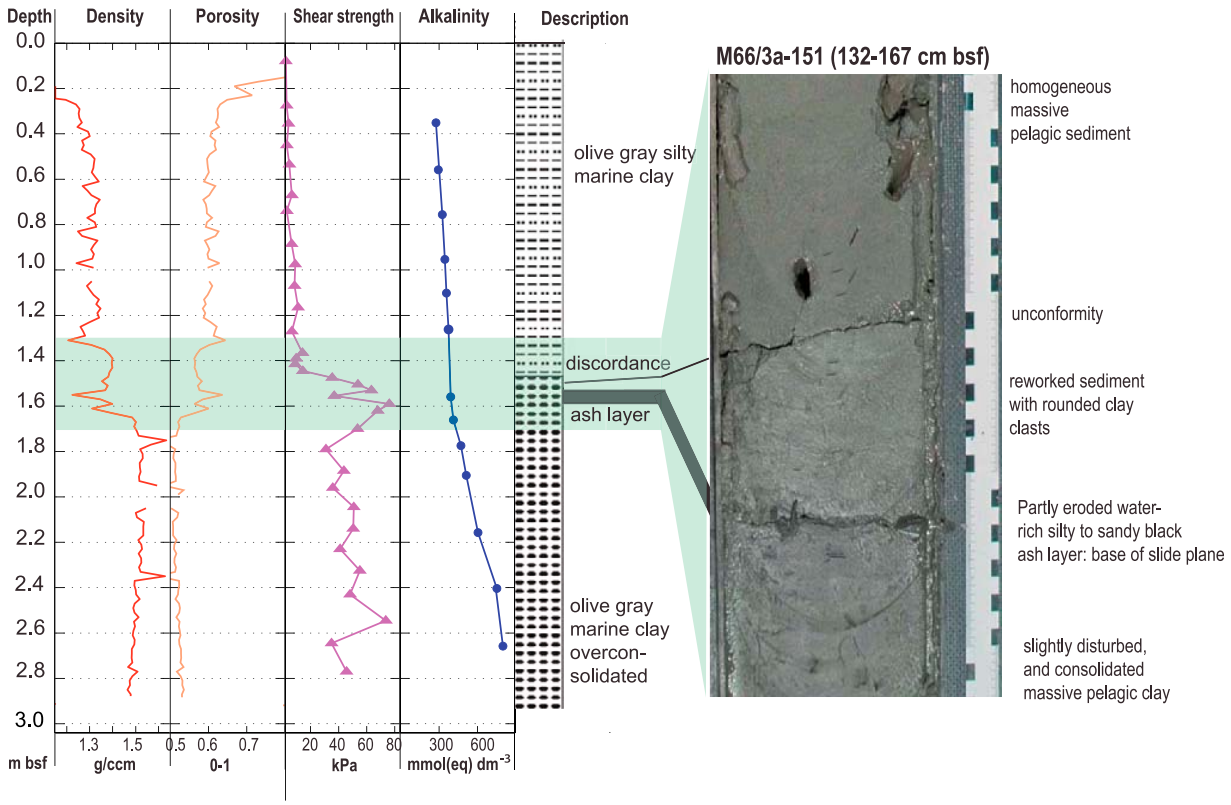

Figure 7. Multisensor core logger data and analog measurements of density, porosity, shear strength, and pore water alkalinity as well as lithology from core M66/151 of Hermosa slide.

Table 1 (Sample). Selected Correlative Major and Trace Elements of Marine and On-Land San Antonio Tephra in Comparison to Other Possible On-Land Masaya Tephras From *Kutterolf et al.* [2008a][a] [The full Table 1 is available in the HTML version of this article]

Tephra Layer	Number	Na_2O	SiO_2	MgO	FeO_t	Al_2O_3	TiO_2	K_2O	CaO	Y	Nb	Cs
Ticuantepe Lapilli/Masaya Tuff	26/5	2.70 (0.61)	53.82 (1.24)	3.87 (1.00)	12.73 (1.97)	15.04 (1.66)	1.39 (0.25)	1.43 (0.24)	8.49 (0.83)	28.26 (0.93)	4.28 (0.07)	0.87 (0.07)
Masaya Triple Layer	96/4	2.82 (0.30)	52.52 (0.55)	4.34 (0.29)	13.46 (0.55)	14.44 (0.40)	1.51 (0.09)	1.47 (0.10)	9.06 (0.32)	32.47 (0.82)	4.79 (0.22)	0.96 (0.02)
La Concepcion Tephra	80/5	2.83 (0.34)	51.58 (0.77)	4.68 (0.68)	13.57 (0.93)	14.69 (0.71)	1.54 (0.20)	1.43 (1.31)	9.28 (0.78)	28.21 (2.21)	4.08 (0.17)	1.02 (0.07)
Fontana Tephra	98/13	3.07 (0.42)	54.51 (4.06)	3.81 (1.08)	12.11 (2.00)	14.91 (0.63)	1.24 (0.25)	1.56 (0.63)	8.36 (1.58)	29.26 (2.00)	3.72 (0.13)	1.10 (0.06)
San Antonio Tephra	98/5	2.90 (0.38)	52.41 (1.61)	4.59 (0.89)	12.96 (1.27)	14.97 (0.82)	1.23 (0.16)	1.37 (0.30)	9.04 (1.01)	24.78 (0.50)	2.89 (0.07)	0.88 (0.02)
M54-11/20-20	32/1	3.00 (0.15)	52.71 (1.04)	4.27 (0.50)	12.64 (0.41)	15.16 (0.22)	1.35 (0.11)	1.43 (0.21)	8.89 (0.67)	25.10 (-)	3.15 (-)	0.88 (-)
M66-167/95-105	35/6	2.94 (0.53)	52.40 (0.88)	4.24 (0.53)	13.15 (1.20)	15.29 (0.80)	1.21 (0.19)	1.35 (0.23)	9.02 (0.61)	23.60 (3.86)	2.24 (0.32)	0.88 (0.13)
M66-151/156-157	21/6	3.18 (0.38)	52.29 (0.84)	4.15 (0.62)	12.22 (1.66)	16.25 (1.64)	1.10 (0.21)	1.05 (0.23)	9.31 (0.93)	21.54 (1.05)	2.44 (0.42)	0.89 (0.15)

[a]Other source areas are excluded due to different trace element compositions and relative stratigraphic order [*Kutterolf et al.*, 2008a]. Number in parentheses shows deviation of single measurements. Number, single measurements per tephra at EMP and LA-ICP-MS.

means that the system is not in balance or in "steady state." Pronounced changes in sedimentary conditions are well known to substantially affect diagenetic processes in marine sediments [e.g., *Thomson et al.*, 1984; *Wilson et al.*, 1986; *Riedinger et al.*, 2005]. Hence, the sharp increase of the alkalinity profile below the mafic ash layer may be indicative for the emplacement of a young sediment unit on top of older strata separated by a discordance, which relates to the slide event.

[26] In line with this interpretation, density, porosity and shear strength profiles also show different trends below and above the mafic ash layer (Figure 7). Above the ash layer density and shear strength values abruptly decrease, while porosity increase.

[27] The 10 cm thick section above the mafic ash layer is made of reworked material containing mafic ash lenses, rounded clay clasts, and carbonatic clay clasts (Figure 7). Within this reworked section, density and shear strength values decrease upward, but are considerably higher than the values in the overlying material. The reworked section is separated from the overlying section by an abrupt change in sediment properties across a discontinuity marked in the core by a crack (possibly secondary in origin and caused by separation at the lithological contact during core recovery). The uppermost section extends up to the seafloor and consists mainly of undisturbed, unconsolidated, water-rich clay. The low alkalinity, shear strength, and density values of this uppermost section clearly suggest that it represents the most recent, post-failure hemipelagic sediment accumulation. Visual inspection support that, in spite of minor disturbance by bioturbation, these clays are mechanically undisturbed and not reworked. On the basis of the physical and geochemical properties (Figure 7) and visual core analysis we conclude that the mafic ash occurs at the top of a section that is over-consolidated considering its burial depth.

3.3. San Antonio Tephra Layer

[28] Cored tephra layers generally have a sharp basal contact to the underlying pelagic clay and many are normally graded in grain size [*Kutterolf et al.*, 2008a]. Marine ash layers from the Central American Volcanic Arc (CAVA) were chemically correlated with tephras of individual eruptions on land using an established database of bulk rock, mineral and glass compositions and eruptions ages, resulting from extensive field expeditions [*Kutterolf et al.*, 2008a]. Evaluation of the chemical composition of the marine mafic ash layer of core

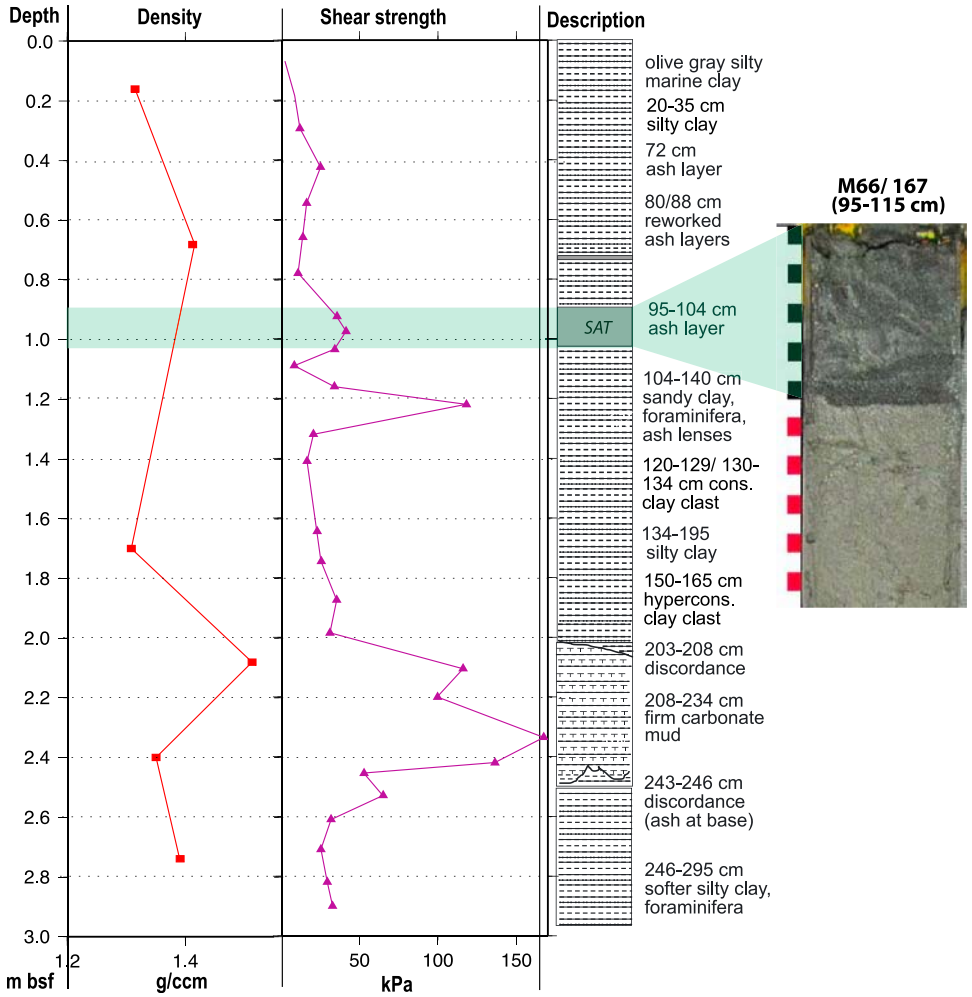

Figure 8. Description and analog data of density and shear strength of core M66/167. The SAT ash layer is marked at 95–104 cm bsf, showing a higher initial shear strength compared to the clay. Note that the overall "normal" trend of the data (increase of shear strength and density with increasing core depth) and peaks in density and shear strength are due to overconsolidated clay clasts or overconsolidated material extruded by the mud mound (Mound Culebra [see also *Kutterolf et al.*, 2008d]).

M66/151 (Table 1 and Figure 7) through EMP and La-ICP-MS analysis revealed that it matches the ~6 ka San Antonio Tephra (SAT) [see also *Kutterolf et al.*, 2008a, 2008c] from the Masaya Caldera [*Peréz and Freundt,* 2006; *Kutterolf et al.*, 2007b]. The SAT was erupted during a plinian eruption that injected volcanic material up to 27 km into the stratosphere where it was transported with the prevailing strong winds toward the Southwest. Therefore deposits of this eruption can be found up to 300 km from its source in the Pacific Ocean and contribute strongly to a calculated erupted tephra volume of ~13.5 km^3 [*Kutterolf et al.*, 2007b, 2008a, 2008b]. The isopaches map of the SAT [*Kutterolf et al.*, 2008b] indicated that it should be 3–6 cm thick within the vicinity of core M66/151, but it is 0.5 cm thick.

[29] We compared chemical analysis of the potential SAT, its grain size distribution, and layer thickness found in the two other offshore cores closest to core M66/151. The most comparable cores, bearing the SAT are M66/167 and M54/11-2 (Figures 1, 8, and 9 and Table 1), taken at roughly similar distances from the Masaya Caldera and from core M66/151 [see also *Kutterolf et al.*, 2008a]. Core M66/167 (Figure 8) was taken at the continental slope, on the flank of a large fluid escape structure named Mound Culebra [*Sahling et al.*, 2008], 160 km northwest of core M66/151 (Figure 1) and 50 km closer to the Masaya volcano. In this core, the SAT was normally graded, 10 cm thick and found at 95–105 cm bsf. Core M54/11-2 (Figures 1 and 9) was taken from the oceanic plate at 200 km distance to the Masaya volcano, 200 km

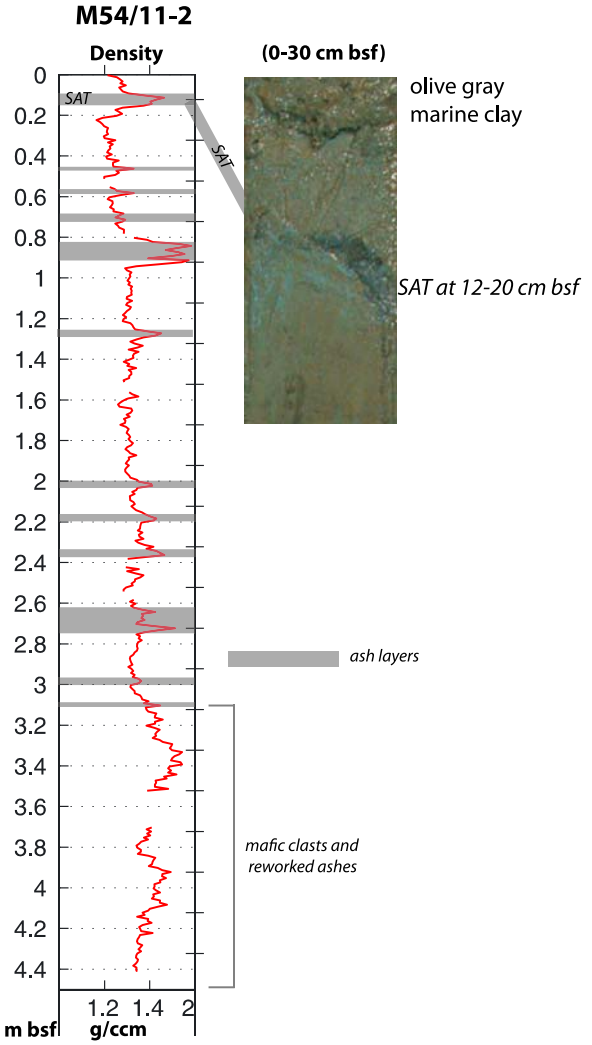

Figure 9. Multisensor core logger data of density and location of ash layers (highlighted in gray) of core M54/11-2 taken from the ocean plate (see also Figure 1 for core location). The SAT ash layer is marked at 12–29 cm bsf (locations of ash layers taken from *Kutterolf et al.* [2007a, Figure 4]).

northwesterly of core M66/151 at Hermosa slide and consisted of a normally graded, 8 cm thick SAT at 12–20 cm bsf. We applied grain size analyses for both cores with a laser particle analyzer, with three repetition measurements per sample and plotted the results as cumulative grain size distribution curves (Figure 10). The distance to the volcano of core M54/11-2 and core M66/151 at Hermosa slide are similar, so that both sites should have the same thickness and grain size distribution. A grain size analysis through wet sieving of the SAT in core M66/151 (Figure 10) demonstrates that the finer top fraction is completely missing and the coarser grained base is only 0.5 thick, which may well be explained by erosion due sliding.

[30] Since the grain size decay is proportional to the thickness decay two arguments support that at Hermosa slide 3–9 cm (80–95%) of the SAT is missing due to the sliding event: Cores close to core M66/151, but outside the failure area, contain a 8–10 cm thick ash layer and finally the regional isopach map indicates at a 3–6 cm thick SAT layer at the location.

3.4. A Model of Sliding at Hermosa Slide Scarp

[31] According to the age of the SAT, the cored slide event must be younger than 6 ka [*Kutterolf et al.*, 2008a, 2008c]. Considering the thickness of 130 cm of undisturbed sediment above the reworked material, and applying sediment accumulation rates of 30–40 cm kyr^{-1} [*Kutterolf et al.*, 2008c], the slide should have occurred about 3700 ± 540 years ago. And it removed about 60–70 cm of sediment, deposited during the previous 2300 ± 540 years. Considering the thin sediment section, and comparing this to the 25 m headwall, which represents the total thickness of the Hermosa slide, the core must have recovered deposits of a smaller retrogressive event within the upper region of the main Hermosa Slide. Therefore we interpret that the cored event occurred above of an older Hermosa slide main event, located over the main slide plane.

3.5. Shear Test Experiments

[32] To study the role of tephra layers potentially affecting the shear strength profile of continental slope sediments we tested the mechanical behavior of ashes and compared it with other terrigenous silt and sand material representative of the embedding sediment layers. In particular, we tested whether the particle fabric of ash layers has an effect on the mechanical response to simple shear compared with normal terrigenous sand. In a study of susceptibility for liquefaction of the Fraser River sand, *Wijewickreme et al.* [2005] pointed out that differences in the particle structure may be a controlling factor of the mechanical response of sand under cyclic loading. The hypothesis to test is whether dry ashes may consolidate more, and/or more rapidly than other dry silt and sand material during a standard shear test. Such behavior would indicate that liquefaction is possible in submerged continental slopes. A specific onshore liquefaction

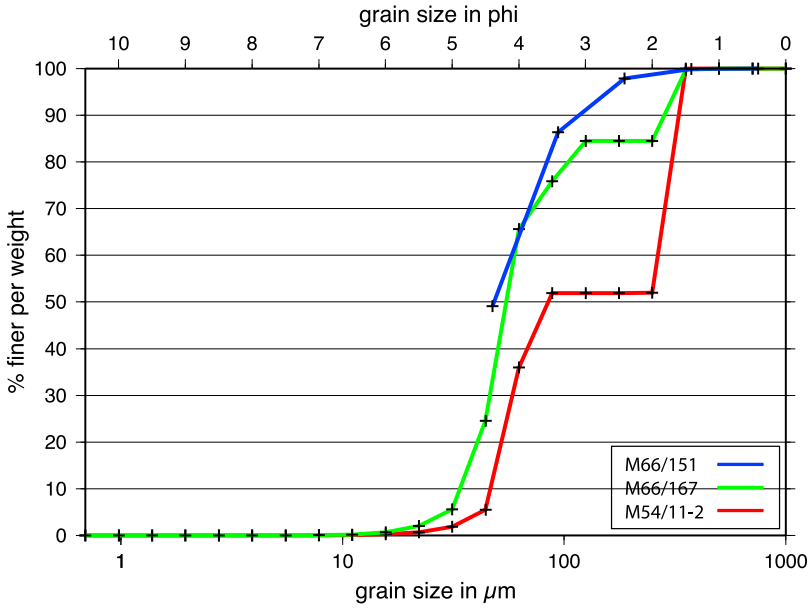

Figure 10. Cumulative grain size distribution curve showing the entire SAT layer of samples M66/151 (grain size <32 not analyzed), M66/167, and M54/11-2. All samples are coarse silt to middle sand (20–600 μm). The k_f values were calculated after *Hazen* [1892], using these curves to determine d_{10} and d_{60} if U < 5 with the formula $k_f = 0.0116 * (d_{10})^2$ and with $U = d_{60}/d_{10}$ and d_y with the value (%) at the grain size (μm) defined along the curve.

mechanism was identified by *National Research Council* (*NRC*) [1985] as "NRC Mechanism B" and is defined as a liquefaction-induced flow failure occurring in loose (not cemented) sand layers overlain by considerably less permeable material, which does not permit drainage during earthquake shaking. For this purpose we measured contractancy (volume reduction) during shearing.

[33] To obtain measurements that span a range of material present in the slope, we used samples not only from the cored SAT layer, but also from other marine mafic and felsic ashes, as well as tephras sampled on onshore deposits. We used samples with a grain shape and grain size distribution similar to the SAT. The samples were collected during *Meteor* cruise M66 and *Sonne* cruise SO173 on the continental slope off Nicaragua, and onshore from the Tierra Blanca Joven deposit in El Salvador.

[34] Examination under optical microscope showed that most tephras, including the SAT, consist of disc-shaped mafic glass shards. To evaluate the influence of grain shape on contractancy, tests were conducted using two different materials: One set of samples composed of disc-shaped felsic or mafic ash grains from Central America and a second set of samples of rounded quartz grains, with a grain size distribution similar to the ashes. Clay was not tested because its cohesive properties and low hydraulic conductivity do not allow fast settlement in water-saturated conditions and will not present a similar layer structure.

[35] We set up a simple dry shear test with a 163 cm^3 shear box with a shear surface of 39.4 cm^2. Tests were run with dry samples of mafic and felsic ashes, and quartz grains of a sand-to-silt fraction. Initial dry bulk densities were calculated from the sample weight filling the box volume. Volume reduction together with an increase in bulk density from shearing results from the contractancy (negative dilatancy) of materials.

[36] Tests were done using sizes ranging between 63 and 125 μm, and 125–250 μm corresponding to the first and second most abundant fraction in the SAT layer. Mafic and felsic ashes with 63–125 μm grain size have initial dry bulk densities of 1.06 g cm^{-3} and 1.2 g cm^{-3}, respectively. The quartz grains of the same fraction have initial dry bulk densities of about 1.6 g cm^{-3} indicating that rounded particles initially build up a denser grain framework. (These results are not caused by the material densities: Quartz has a material density of 2.65 g cm^{-3}, mafic glass has the highest material density of 2.75 g cm^{-3} and felsic glass the lowest material density of 2.45 g cm^{-3}.)

[37] Figure 11 shows that ashes have higher contractancy than the reference rounded quartz grains,

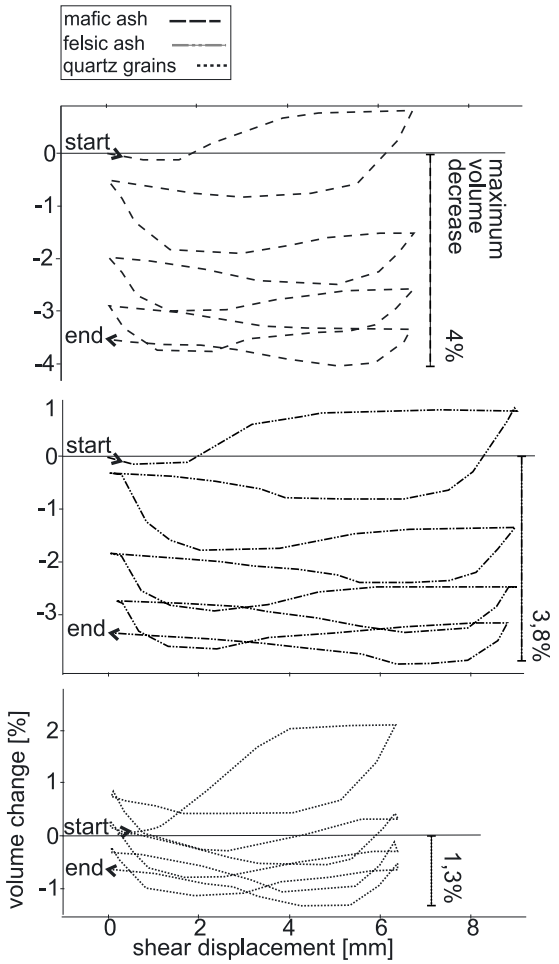

Figure 11. Cyclic direct shear tests showing total volume change in % of mafic and felsic ashes and quartz grains of 0.063–0.125 mm grain size. Shearing went from left to right, continued until no further volume changes were recorded, and sheared back to the left (arrows). For each sample four cycles of shearing were conducted (effective vertical stress is 40 kPa ~7 m below seafloor, and shear velocity is 0.5 mm/min).

as could be expected from their initial lower bulk densities. Tests using the most abundant ash grain size (63–125 μm silt to fine sand) show a volume reduction 3 times higher than for quartz grains (Figure 11). Tests using the second most abundant grain size (125–250 μm, fine to middle sand) show a volume reduction 8.5 times larger than for quartz grains. A rearrangement of subvertically orientated laminar ash shards into subhorizontal attitudes would explain the much higher rates of volume reduction compared to rounded particles of the quartz sand. Thus, tests indicate that ash layers may undergo an anomalously high volume reduction of their grain skeleton compared to any other typical slope sediment, including quartz-rich terrigenous sand or silt layers discretely interbedded within clay. Although our tests did not include tests with pressure waves simulating earthquake shaking on the slope, we interpret that the differences in compaction of the samples will also occur during shaking on the slope by earthquakes.

3.6. High Hydraulic Conductivities of the SAT Layer

[38] Coarser tephra material sandwiched in between very fine grained clayey sediment of the continental slope should create layers of high permeability. Therefore, we estimated hydraulic conductivities of the SAT in the three cores by means of the grain size distribution curves after *Hazen* [1892]. This is a simple method to estimate the hydraulic conductivity, because it gives values similar compared to pump experiments, if the soil is not too inhomogeneous (U < 5, where U is the unconformity index given as the quotient of the grain sizes corresponding to the 60% and the 10% intersection with the cumulative grain size curve). Because of its simplicity and reliability, this method is still routinely applied in hydrogeology [*Hoelting and Coldewey,* 2009] (for details of equation see caption of Figure 10). Following, hydraulic conductivities (k_f value) for the SAT layer were calculated: in core M66/151 it has a $k_f \sim 2.6 \times 10^{-5}$ m s^{-1} (due to the very little amount of tephra within core M66/151 this is only an indication), in core M66/167 it has a $k_f = 1.75 \times 10^{-5}$ m s^{-1}, and in core M54/11 it has a $k_f = 3.4 \times 10^{-5}$ m s^{-1} (Figure 10). All values are in the range of 10^{-5} m s^{-1}, which is consistent with published values for permeable coarse silt to middle sand [*Deutsches Institut für Normung,* 2003].

[39] Since the SAT layer is normally graded we also estimated k_f values for the lower, coarser part of the layer, and for the upper, finer part (for cores M66/167 and M54/11-2). We estimated a k_f of 6.6×10^{-4} m s^{-1} for the coarser part of sample M54/11-2, within the grain size range of 1000–250 μm, (making up 48% of the entire layer) (Figure 12). A similar value of $k_f = 3.6 \times 10^{-4}$ m s^{-1} for the grain size range 1000–176.7 μm, (making up 15.53% of the entire layer) was estimated for sample M66/167 (Figure 12). These k_f values are about one magnitude higher than the values estimated for the entire layer, which implies a much higher permeability in the coarser basal part of the ash layer.

[40] The finer parts of both samples have k_f values of magnitude 10^{-5}; 3.07×10^{-5} m s^{-1} for sample M54/11-2 within the grain size range 176.7–0.69 μm (constituting 51.53% of the ash layer (Figure 13)

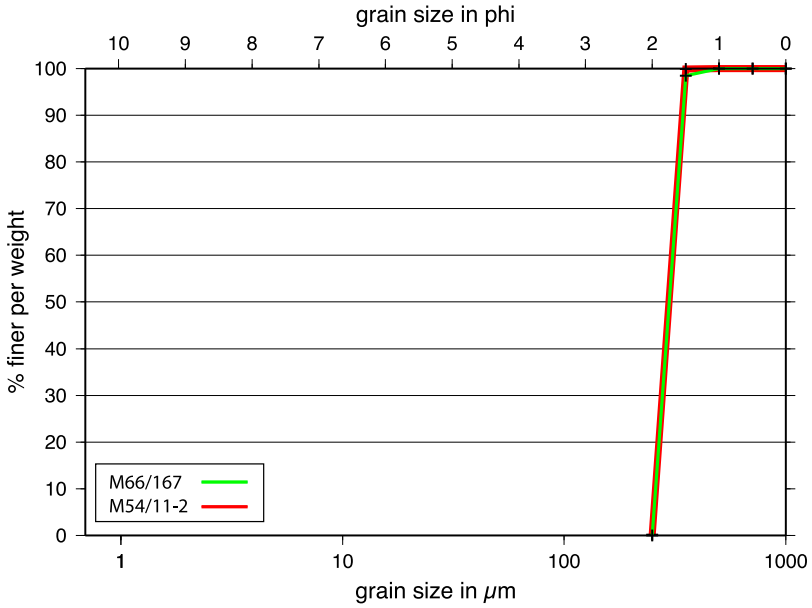

Figure 12. Cumulative grain size distribution of the coarser part of the SAT layer from cores M66/167 and M54/11-2, using the same method for k_f calculation described in Figure 10.

and for M66/167 $k_f = 1.16 \times 10^{-5}$ m s^{-1} for the grain size range of 125–0.69 μm (making up 84% of the layer) (Figure 13). Therefore, the hydraulic conductivity values of the SAT calculated from the grain size distribution suggest that the layer is highly permeable in comparison to other slope sediment, with higher permeability in its coarser basal lower part. These k_f values are similar to values of onshore aquifers [*Hoelting and Coldewey*, 2009].

3.7. Tephra Layers as Slide Planes: Conceptual Model

[41] Tephra layers contain disc-shaped ash particles that have accumulated by a different settling behavior than terrigenous clay sediments of the slope. After a volcanic eruption the ash is transported by winds and settles through the water column producing well-sorted deposits in just hours to a few days [*Fisher,* 1965; *Carey,* 1997]. Ash particles reach the seafloor in convective plumes that build dense particle-rich currents that move at least one order of magnitude faster than predicted by Stokes's law [*Carey,* 1997]. Therefore, the resulting deposit is not only well sorted, but also it bears the characteristics of random orientation of the disc-shaped volcanic shards. The resulting tephra is built by a rigid skeleton and large water-filled pore spaces, resulting in a hydraulically conductive layer. Such highly porous, highly conductive, 1–15 cm thick ash layers are intercalated within ~1 m thick clay units in the cores retrieved from the slides. In contrast, the clay-rich material, dominant on the slope, forms a water-retaining unit due to its low hydraulic conductivity.

[42] Shearing of ashes causes a high volume contraction that is produced by the rearrangement of the disc-shaped grain particles. We hypothesize that a significant difference in the rearrangement of particles along a shear plane may be expected during seismically induced shaking. Such a difference in rearrangement may cause proportionally different volumetric changes depending on the composition of single layers or may even occur within specific layers, with ash layers undergoing the largest contractancy.

[43] Shaking by large magnitude earthquakes of may force ash layers with noncohesive properties to undergo a sudden major grain rearrangement. The high hydraulic conductivity and relatively low bulk density of ashes, compared to the embedded terrigenous silt-sand, allow this process to occur under undrained conditions. Volume reduction will change the vertical profile of the shear strength of the ash layer: Grains settle toward the bottom of the layer where porosity rapidly decreases, and would be replaced by water in the middle to upper portion of the layer (Figure 14). The shear strength in the upper portion of the ash layer will suddenly decrease promoting the creation of a weak detachment plane. In extreme cases a water interlayer may be formed beneath the less permeable material.

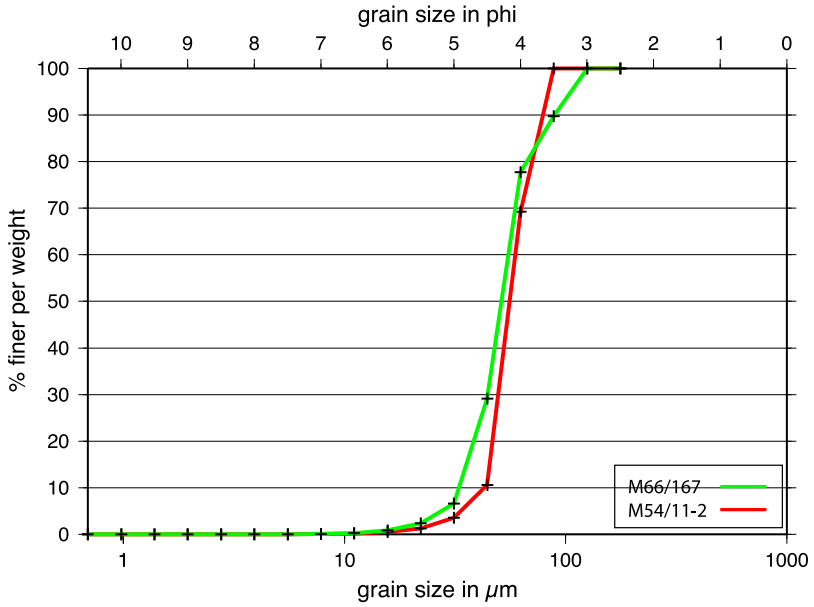

Figure 13. Cumulative grain size distribution of the finer part of the SAT layer from cores M66/167 and M54/11-2, using the same method for k_f calculation described in Figure 10.

Since the water interlayer would have zero shear strength a failure could easily occur.

4. Slides and Seismicity

[44] In addition to the contractancy and shear strength loss that could initiate sliding according to our hypothesis, individual tephra layer properties including thickness, lateral continuity and specific grain properties such as grain size, grain shape, degree of alteration, etc. may also influence the magnitude of the loss of shear strength during shaking. Our hypothesis is that the mafic ash layer of core M66/151 underwent liquefaction similar to the onshore NRC Mechanism B [*NRC*, 1985] inducing flow failure under undrained conditions.

[45] Comparing the number of large translational slides with the occurrence of large earthquakes offshore Costa Rica and Nicaragua (~15 earthquakes of Ms > 7 in last ~100 years, after *Ambraseys and Adams* [1996]), and considering the amount of time that the hemipelagic sediment accumulation rates of 30–40 cm kyr^{-1} [*Kutterolf et al.*, 2008c] require to fill tens of meters high slide scarps, it becomes clear that not each large earthquake causes a large slide. The largest headwall thickness at Masaya slide (Figures 1 and 3) is around 160 m. Applying sedimentation rates of 30–40 cm kyr^{-1} such a scarp would be filled in a time period of ~450,000 years. Therefore, we propose that the large Masaya and neighboring slides are less than ~450,000 years old, and in the case where sediment has not in filled the scars noticeably they are probably much younger. Large earthquakes (>7 Ms) occur along each segment of the margin with a 50–100 year recurrence time [*Ambraseys and Adams,* 1996], indicating that each area goes

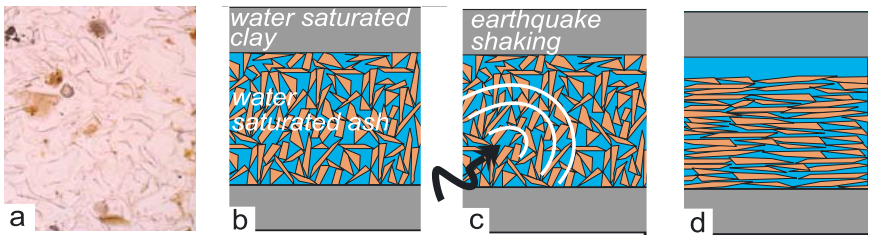

Figure 14. (a) Microscope photography of horizontally spread felsic ash shards (grain size is 63–125 μm). (b) Cartoon of a vertical cut through fresh deposited ash before an earthquake. (c) Earthquake shaking cancels grain-to-grain contact, which decreases the shear strength of the ash layer. (d) In the end-member case an interlayer may form during shaking.

through many earthquake cycles before sliding in a large event. This observation may indicate that besides the presence of ash layers the initiation of large-scale sliding is controlled by several conditions within the slope sediment, for instance the depth of penetration and the lateral extent of fault scarps within the slope, where many headwalls of the slides appear to initiate. However, core M66/151 recovered sediments indicative for a small-scale event, which is not visible with the resolution of our data. Hence, we interpret that small-scale slumping is more common than large-scale slumping. According to the estimated accumulation rates, the weak layer was less than 1 m depth below the seafloor. Accumulation rates can considerably change along slope, depending on the precise location and the corresponding environmental conditions on the slope. For example, higher accumulation rates must occur at the mouth of a canyon. And we speculate that the cored event removed sediment that was thicker than calculated by accumulation rates, because it is located in front of a canyon (Figures 1 and 2).

[46] Because failure occurs after several earthquake cycles, it is clear that the sediment undergoes several shaking event close to failure. This is important, because silty clays (normal marine sediment) undergoing repeated, nonfailure, seismic events can actually consolidate the sediment column through extrusion of excess pore water during earthquakes [*Locat and Lee,* 2002]. If rearrangement of grains in the ash layer happens abruptly, rather than being a gradual process, the ash layers do not undergo the same sediment strengthening during burial, and the slope strata is formed by layers of strengthened silty clays alternating with weakened ash layers. Thus, in our view the shear strength of clays and ashes follow opposed trends during repeated earthquake shaking.

[47] The behavior of the ash shards may perhaps be comparable to that of siliceous oozes, where the fragile framework of rigid skeletons of diatoms and radiolarians can be easily dissolved or being broken by overburden exceeding a certain threshold, and hence cause sudden porosity reduction and overpressuring of pore water [*Volpi et al.*, 2003, and references therein].

5. Conclusion

[48] Evidence from MSCL-density profiles, physical index properties, and pore water geochemistry indicate that tephra layers may act as weak layers in continental slope sediment and precondition the slope for instability. Our manuscript is based on observations of shallow slumps offshore Central America, where the base of the slide plane is parallel to the surrounding seafloor and the shallow stratigraphy. The proposed slip plane consists of a regionally well-mapped San Antonio tephra layer. Based on the precise age information about the deposition of the tephra and the accumulation rate we calculated the minimum of thickness of material that was removed by the slide. Grain size analysis shows, that the ash is highly conductive to water. Simple shear tests on the ash indicated high compaction rates during shear, leading us to the hypotheses that a sudden compaction due to rearrangement of the grains could produce peak pore pressures and liquefaction of the layer.

[49] The new model proposes that discrete tephra layers of the slope may have a distinct mechanical behavior compared to the more ubiquitous terrigenous slope sediment. The model proposes that the grain framework collapse of highly permeable ash layers during earthquake shaking creates a weak layer that serves as detachment plane for translational sliding.

[50] This scenario is applicable to all convergent margins with active volcanic arcs in geological settings similar to Central America, that occur around the Circum-Pacific, and Indian Ocean subduction zones and perhaps in the Mediterranean sea. Eruptions producing widespread submarine tephra layers also occur on volcanic islands (e.g., Hawaii, Canaries, Azores, Reunion, Cape Verde islands). Similar environments may exist onshore where large arc volcanoes occur within lakes such as in Kamchatka, Mexico, and Central America.

Acknowledgments

[51] This research was supported by the Deutsche Forschungsgemeinschaft as part of the SFB 574 (Sonderforschungsbereich). We thank the crew and captain of the *Meteor* and participants of cruise M66-3 for their help in collecting the cores and onboard measurements. This publication is contribution 136 of the Sonderforschungsbereich 574 “Volatiles and Fluids in Subduction Zones” at Kiel University. We thank C. R. Ranero and U. ten Brink for comments on a previous version of the manuscript and A. Wetzel for discussion. We are also thankful to the journal referees D. Orange and A. Camerlenghi for their constructive reviews.

References

Ambraseys, N. N., and R. D. Adams (1996), Large-magnitude Central American earthquakes, 1898–1994, *Geophys. J. Int.*, *127*, 665–692, doi:10.1111/j.1365-246X.1996.tb04046.x.

Blum, P. (1997), Physical properties handbook: A guide to the ship board measurement of physical properties of deep-sea cores, *Tech. Note, 26*, Ocean Drill. Program, College Station, Tex. (Available at http://www-odp.tamu.edu/publications/tnotes/tn26/INDEX.HTM)

Caress, D. W., and D. N. Chayes (1996), Improved processing of Hydrosweep DS multibeam data on the R/V *Maurice Ewing*, *Mar. Geophys. Res.*, *18*, 631–650, doi:10.1007/BF00313878.

Carey, S. (1997), Influence of convective sedimentation on the formation of widespread tephra fall layers in the deep sea, *Geology*, *25*(9), 839–842, doi:10.1130/0091-7613(1997)025<0839:IOCSOT>2.3.CO;2.

Castro, G. (1969), *Liquefaction of Sands*, *Harvard Soil Mech. Ser.*, vol. 87, Harvard Univ., Cambridge, Mass.

Deutsches Institut für Normung (2002), Soil, investigation and testing—Determination of shear strength—Part 3: Direct shear test, *Rep. DIN 18137-3*, Berlin.

Deutsches Institut für Normung (2003), Soil, investigation and testing—Determination of the coefficient of water permeability—Part 2: Field tests, *Rep. DIN 18130-1*, Berlin.

Field, M. E., J. V. Gardner, A. E. Jennings, and B. D. Edwards (1982), Earthquake induced sediment failures on a 0.258 slope, Klamath River delta, Calif. *Geol.*, *10*, 542–546.

Fisher, R. V. (1965), Settling velocity of glass shards, *Deep Sea Res.*, *12*, 345–353.

Graham, J. (1984), Methods of stability analysis, in *Slope Instability*, edited by B. Brunsdan and D. B Prior, pp. 171–215, John Wiley, New York.

Hampton, M. A., and H. J. Lee (1996), Submarine landslides, *Rev. Geophys.*, *34*, 33–59, doi:10.1029/95RG03287.

Hansbo, S. (1957), A new approach to the determination of the shear strength of clay by the fall-cone test, *Proc. R. Swed. Geotech. Inst.*, *14*, 5–47.

Hazen, A. (1892), Some physical properties of sand and gravels with special reference to their use in filtration, *Annu. Rep.*, 24, pp. 541–556, Mass. State Board of Health, Boston.

Hensen, C., M. Zabel, K. Pfeifer, T. Schwenk, S. Kasten, N. Riedinger, H. D. Schluz, and A. Boetius (2003), Control of sulfate pore-water profiles by sedimentary events and the significance of anaerobic oxidation of methane for the burial of sulfur in marine sediments, *Geochim. Cosmochim. Acta*, *67*(14), 2631–2647, doi:10.1016/S0016-7037(03)00199-6.

Hoelting, B., and W. G. Coldewey (2009), *Hydrogeologie-Einfuehrung in die allgemeine und angewandte Hydrogeologie*, 7th ed., 383 pp., Spektrum Akad., Heidelberg, Germany.

Houlsby, G. T. (1982), Theoretical analysis of the fall cone test, *Geotechnique*, *32*, 111–118, doi:10.1680/geot.1982.32.2.111.

Karlsrud, K., and L. Edgers (1982), Some aspects of submarine slope stability, in *Marine Slides and Other Mass Movements*, *NATO Conf. Ser. IV, Mar. Sci.*, vol. 6, edited by S. Saxov and J. K. Nieuwenhuis, pp. 68–81, Plenum, New York.

Kokusho, T. (2003), Current state of research on flow failure considering void redistribution in liquefied deposits, *Soil. Dyn. Earthquake Eng.*, *23*, 585–603, doi:10.1016/S0267-7261(03)00067-8.

Kutterolf, S., U. Schacht, H. Wehrmann, A. Freundt, and T. Moerz (2007a), Onshore to offshore tephrostratigraphy and marine ash layer diagenesis in Central America, in *Central America Geology, Resources and Hazards*, vol. 2, edited by J. Buntschuh and G. E. Alvarado, pp. 395–423, A. A. Balkema, Lisse, Netherlands.

Kutterolf, S., A. Freundt, W. Peréz, H. Wehrmann, and H. U. Schmincke (2007b), Late Pleistocene to Holocene, temporal succession and magnitudes of highly explosive volcanic eruptions in west-central Nicaragua, *J. Volcanol. Geotherm. Res.*, *163*, 55–82, doi:10.1016/j.jvolgeores.2007.02.006.

Kutterolf, S., A. Freundt, W. Perèz, T. Moerz, U. Schacht, H. Wehrmann, and H. -U. Schmincke (2008a), Pacific offshore record of plinian arc volcanism in Central America: 1. Along-arc correlations, *Geochem. Geophys. Geosyst.*, *9*, Q02S01, doi:10.1029/2007GC001631.

Kutterolf, S., A. Freundt, and W. Peréz (2008b), Pacific offshore record of plinian arc volcanism in Central America: 2. Tephra volumes and erupted masses, *Geochem. Geophys. Geosyst.*, *9*, Q02S02, doi:10.1029/2007GC001791.

Kutterolf, S., A. Freundt, U. Schacht, D. Buerk, R. Harders, T. Moerz, and W. Perèz (2008c), Pacific offshore record of plinian arc volcanism in Central America: 3. Application to forearc geology, *Geochem. Geophys. Geosyst.*, *9*, Q02S03, doi:10.1029/2007GC001826.

Kutterolf, S., V. Liebetrau, T. Mörz, A. Freundt, T. Hammerich, and D. Garbe-Schönberg (2008d), Lifetime and cyclicity of fluid venting at fore arc mound structures determined by tephrostratigraphy and radiometric dating of authigenic carbonates, *Geology*, *36*(9), 707–710, doi:10.1130/G24806A.1.

Locat, J., and H. J. Lee (2002), Submarine landslides: Advances and challenges, *Can. Geotech. J.*, *39*, 193–212, doi:10.1139/t01-089.

McIntosh, K. D., E. A. Silver, I. Ahmed, A. Berhorst, C. R. Ranero, R. K. Kelly, and E. R. Flueh (2007), The Nicaragua convergent margin: Seismic reflection imaging of the source of a tsunami earthquake, Costa Rica, in *The Seismogenic Zone of Subduction Thrust Faults*, edited by T. Dixon and J. C. Moore, pp. 257–287, Columbia Univ. Press, New York.

Mulder, T., and P. Cochonat (1996), Classification of offshore mass movements, *J. Sediment. Res.*, *66*, 34–57.

National Research Council (NRC) (1985), *Liquefaction of Soils During Earthquakes*, 240 pp., Natl. Acad. Press, Washington, D. C.

Peréz, W., and A. Freundt (2006), The youngest highly explosive basaltic eruptions from Masaya caldera (Nicaragua): Stratigraphy and hazard assessment, in *Volcanic Hazards in Central America*, edited by W. I. Rose et al., *Spec. Pap. Geol. Soc. Soc. Am.*, *412*, 189–207.

Ranero, C. R., and R. von Huene (2000), Subduction erosion along the Middle America convergent margin, *Nature*, *404*, 748–752, doi:10.1038/35008046.

Ranero, C. R., I. Grevemeyer, H. Sahling, U. Barckhausen, C. Hensen, K. Wallmann, W. Weinrebe, P. Vannucchi, R. von Huene, and K. McIntosh (2008), Hydrogeological system of erosional convergent margins and its influence on tectonics and interplate seismogenesis, *Geochem. Geophys. Geosyst.*, *9*, Q03S04, doi:10.1029/2007GC001679.

Riedinger, N., K. Pfeifer, S. Kasten, J. F. K. Garming, C. Vogt, and C. Hensen (2005), Diagenetic alteration of magnetic signals by anaerobic oxidation of methane related to a change in sedimentation rate, *Geochim. Cosmochim. Acta*, *69*, 4117–4126, doi:10.1016/j.gca.2005.02.004.

Sahling, H., D. G. Masson, C. R. Ranero, V. Hühnerbach, W. Weinrebe, I. Klaucke, D. Bürk, W. Brückmann, and E. Suess (2008), Fluid seepage at the continental margin offshore Costa Rica and southern Nicaragua, *Geochem. Geophys. Geosyst.*, *9*, Q05S05, doi:10.1029/2008GC001978.

Skempton, A. W., and J. N. Hutchinson (1969), Stability of natural slopes and embankment foundations: State-of-the-art report, *Proc. Int. Conf. Soil Mech. Found. Eng. 7th*, *2*, 291–335.

Spangenberg, T. (2002), Erdbeben-Hangrutschungen-Tsunami: Beitraege zum Verstaendnis zur Subduktion vor Nicaragua und zu den komplexen Beziehungen zwischen Erdbeben, gravitativen Massenverlagerungen und Tsunamigenerierung, Ph.D. thesis, 233 pp., Ernst-Moritz-Arndt Univ. Greifswald, Greifswald, Germany.

Thomson, J., T. R. S. Wilson, F. Culkin, and D. J. Hydes (1984), Non-steady state diagenetic record in eastern equatorial Atlantic sediments, *Earth Planet. Sci. Lett.*, *71*, 23–30, doi:10.1016/0012-821X(84)90049-9.

Volpi, V., A. Camerlenghi, C. -D. Hillebrand, M. Rebesco, and R. Ivaldi (2003), Effects of biogenic silica on sediment compaction and slope stability on the Pacific margin of the Antarctic Peninsula, *Basin Res.*, *15*, 339–363, doi:10.1046/j.1365-2117.2003.00210.x.

von Huene, R., C. R. Ranero, and W. Weinrebe (2000), Quaternary convergent margin tectonics of Costa Rica, segmentation of the Cocos Plate, and Central American volcanism, *Tectonics*, *19*, 314–334, doi:10.1029/1999TC001143.

von Huene, R., C. R. Ranero, and P. Watts (2004), Tsunamigenic slope failure along the Middle America Trench in two tectonic settings, *Mar. Geol.*, *203*, 303–317, doi:10.1016/S0025-3227(03)00312-8.

Wessel, P., and W. H. F. Smith (1998), New improved version of generic mapping tools released, *Eos Trans. AGU*, *79*, 579, doi:10.1029/98EO00426.

Wijewickreme, D., S. Sriskandakumar, and P. Byrne (2005), Cyclic loading response of loose air-pluviated Fraser River sand for validation of numerical models simulating centrifuge tests, *Can. Geotech. J.*, *42*, 550–561, doi:10.1139/t04-119.

Wilson, T. R. S., J. Thomson, D. J. Hydes, S. Colley, F. Culkin, and J. Sørensen (1986), Oxidation fronts in pelagic sediments: Diagenetic formation of metal-rich layers, *Science*, *232*, 972–975, doi:10.1126/science.232.4753.972.

Zabel, M., and H. D. Schulz (2001), Importance of submarine landslides for non-steady state conditions in pore-water systems—Lower Zaire (Congo) deep-sea fan, *Mar. Geol.*, *176*, 87–99, doi:10.1016/S0025-3227(01)00164-5.